ILASS 2008
Sep. 8-10, 2008, Como Lake, Italy

Paper ID ILASS08-9-3

NUMERICAL SIMULATION OF SINGLE DROP IMPINGEMENT ONTO A PLANE LIQUID SURFACE

Tomio Okawa

Department of Mechanical Engineering, Osaka University
Phone: +81-6-6879-7257, Fax: +81-6-6879-7247
E-mail: t-okawa@mech.eng.osaka-u.ac.jp

ABSTRACT
Systematic numerical simulations were carried out to investigate the effects of target film thickness and impingement angle on the process of crown formation following the single drop impingement. A part of liquid originally included in the inner region of crown was transported to the outer region when the liquid film was thick, while the liquid transport was negligible for sufficiently thin films. Inhibition of liquid transport resulted in a rise of impact pressure, an increase in liquid velocity in a crown wall, and a decrease in crown wall thickness. This suggested that the reduction of film thickness leads to an enhancement of splashing of secondary drops since the crown wall is destabilized. It was also confirmed that the pressure rise at the bottom wall is mitigated noticeably if the target liquid film is sufficiently thick. In the case of oblique impact, not only the normal component but also the tangential component of impact velocity was influential in determining the impact pressure and the liquid velocity in a liquid sheet formed during the impact process. This was considered one of the main reasons that the deposition-splashing limit is not dominated by the normal component but the total momentum vector of impact velocity. It was also shown that the elongation of liquid sheet is restricted in the case of very oblique impact since the liquid sheet is directed downward and hence collides with the surface of target liquid film.

INTRODUCTION

If a single drop impacts on a plane liquid film, a crown-like fascinating liquid structure is formed on the film surface and then many secondary drops are splashed from the crown rim provided the size or the velocity of primary impacting drop is sufficient [1]. This splashing event is not only the subject of fundamental scientific interest but of great relevance to many technical applications. Examples include combustible fuel injection in engines, surface cooling by liquid sprays, ink-jet printing, atomization of dangerous liquids, dryout of liquid film in diabatic annular two-phase flows and sound detection in ocean under rainfall [2–5].

The condition for the splashing to take place during the normal drop impact was hence explored experimentally by many researchers [6–9]. From these studies, the impact K-number is considered one of the most promising parameters to characterize the deposition-splashing limit; here, K is calculated from the impact Weber number We and the Ohnesorge number Oh by $K = WeOh^{-0.4}$. However, since the experimental information on the total mass of secondary drops and the effect of impingement angle was scarce, the present author measured the total secondary-to-incident mass ratio for both normal and oblique impacts [10, 11]. The effect of liquid flow in the target liquid film on the outcome of collision was also investigated [12]. It was found that the effect of the impingement angle on the critical value of K is not significant if the total momentum vector is used in calculating We but it is remarkably influential in the total mass of secondary drops.

When droplets impinge on a solid surface, the local pressure at the impact point can be considerably high. It is however expected that the damage of solid material is mitigated if the target surface is covered by a sufficiently thick liquid film. This implies that the drop impact on a liquid film is also closely associated with the erosion problem such as the soil erosion by rainfall [13, 14] and the erosion of wall material by water drop impingement in some energy generation systems [15].

In order to understand the mechanism of splashing and the erosion damage induced by the drop impact, detailed information on the local instantaneous hydraulic conditions in liquid is indispensable. To this end, however, numerical rather than experimental approach is considered useful since the measurement of local instantaneous parameters within liquid is extremely difficult. Furthermore, with the recent improvements of computer performance, some researchers carried out sophisticated numerical simulations and succeeded to reproduce the complex flow structure formed following the drop impact [16–21].

In view of this, in the present work, systematic numerical simulations are carried out to investigate the effects of several important parameters on the process of single drop impingement onto a plane liquid film. If the size or the velocity of the primary impacting drop is sufficient, a small liquid jet is formed at the neck region between the impacting drop and the target liquid surface immediately after the impact and then it develops into the liquid crown. In determining the onset of splashing and the total mass of secondary drops, the local pressure at the neck region and the fluid velocity in the liquid jet are considered of importance [19]. Also, the erosion damage induced by the drop impingement would become significant with an increase in the pressure rise on the solid surface. Thus, particular attention is paid to the pressure distribution and the jet velocity in this work. The numerical results are used to interpret the available experimental data concerning the splashing event and to investigate the mitigation of erosion damage by the presence of liquid film.

NUMERICAL METHOD

The initial and boundary conditions of the present numerical simulation are shown schematically in Fig. 1. Since time-consuming three-dimensional computation is necessary to simulate the production process of secondary drops, it was decided to perform two-dimensional simulations for the early instants of impact process preceding the secondary drop production. This simplification enabled to obtain systematic information on the effects of several important parameters on the process of crown formation. The oblique as well as normal impacts were considered in this work. It should however be noted that, since the process of oblique impact is not axisymmetric even in the early instants, not the axisymmetric but rectangular coordinates were used in the case of oblique impact. This implies that the cylindrical drop impacted on the liquid film in the simulations of oblique impact.

The same water-like liquid of constant hydraulic properties was used for the drop and liquid film (density ρ was 1,000 kg/m^3, viscosity μ was 0.001 Pa·s and surface tension σ was 0.07 N/m). The gas of constant properties was used for the surrounding gas (density was 5 kg/m^3 and viscosity was 20 μPa·s). It is noted that the gas density was higher than the air density at atmospheric pressure to avoid numerical instability but it is still much lower than the liquid density. From the experimental data reported in literature [6–12], the impact K-number ($K = WeOh^{-0.4}$), the dimensionless film thickness ($\eta = h/d$) and the impingement angle from the vertical line α were selected as the parameters of primary importance in determining the outcome of collision; here, We is the impact Weber number ($= \rho V^2 d/\sigma$), Oh is the Ohnesorge ($= \mu/(d\sigma\rho)^{0.5}$), h is the film thickness, d is the primary drop diameter and V is the impact velocity.

In the initial condition, the drop was spherical or cylindrical and directed toward the target liquid with the uniform velocity; d was set to 0.4 mm in all the simulations while V and α were varied within 2–20 m/s and 0–70°, respectively. The resulting ranges of We and K were within 23–2,286 and 177–17,720, respectively. Here, not the normal component of V but the total momentum vector was used in calculating We since the total momentum vector was more appropriate to characterize the deposition-splashing limit for oblique impact in our previous experiments [11]. The liquid film and the surrounding gas were stationary in the initial condition and the gravitational acceleration of 9.8 m/s^2 was directed toward the bottom wall. The film thickness h was varied within 0.01–0.4 mm (η = 0.025–1). The initial gap distance between the drop and film was set to 0.04 mm (= 0.1d). The computational domain was 2 mm wide and 1 mm high in the rectangular coordinates but the domain width was reduced to 1 mm in the cylindrical coordinates considering the axial symmetry. The no-slip and constant pressure conditions were applied to the bottom and top boundaries, respectively; here, the pressure at the top was set to the atmospheric pressure P_0. For the side wall, the symmetric and periodic boundary conditions were used in the cylindrical and rectangular coordinates, respectively.

The flow field containing the phase interface was calculated based on the VOF (volume of fluid) method using the commercial code CFX-10.0. Two-dimensional uniform square grids were used in the present simulation. The effect of mesh size Δx on the numerical solution was tested in the reference case ($d = h = 0.4$ mm, $\alpha = 0°$, $V = 10$ m/s, $We = 571$, $K = 4{,}430$). The calculated time-evolutions of gas-liquid interface are depicted in Fig. 2; here, τ denotes the time from the instant of impact in units of d/V ($\tau = Vt/d$) and the darkness is proportional to the liquid volume fraction in each computational cell. As shown in Fig. 2a, if Δx is set to 8 μm, numerical diffusion is rather significant and the formation of liquid jet is not observed in the neck region at $\tau = 0.1$. In the numerical results for $\Delta x = 2$ μm (Fig. 2c), the breakup of liquid sheet is clearly seen at $\tau = 1$; however, this event is not observed at the same time level for $\Delta x = 4$ μm (Fig. 2b). This indicates that the present numerical method requires 2 μm or finer mesh to obtain quantitatively accurate numerical solution. However, from the allowable computation time and the similarity of the crown shapes depicted in Figs. 2b and c, it was assumed that the mesh size of 4 μm is sufficient to obtain fairly good description of the drop impact process.

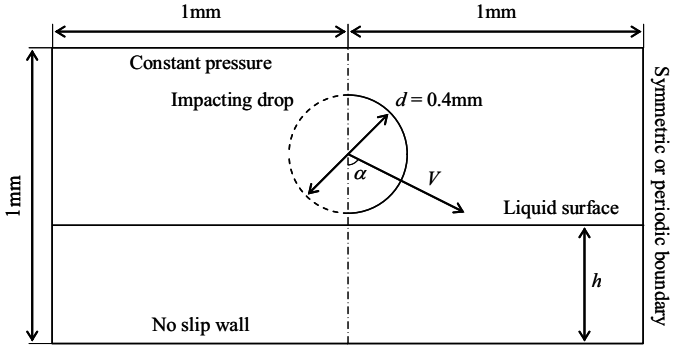

Fig. 1: Schematic diagram of initial and boundary conditions. (Axisymmetric and rectangular coordinates were used for normal and oblique impacts, respectively. Left-half was used only for oblique impacts.)

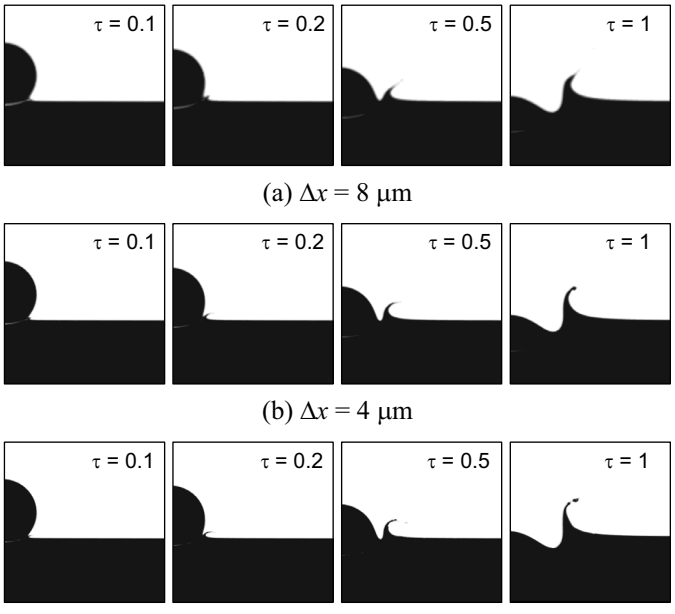

(a) $\Delta x = 8$ μm

(b) $\Delta x = 4$ μm

(c) $\Delta x = 2$ μm

Fig. 2: Effect of mesh size on the time evolution of gas-liquid interface; darkness is proportional to liquid volume fraction.

NUMERICAL RESULTS OF NORMAL IMPACT

Interfacial shape

In the numerical simulations of normal impact, the impact velocity V and the film thickness h were changed parametrically. The effect of V on the calculated interfacial

shape at $\tau = 1$ is displayed in Fig. 3a. It can be seen that the crown wall becomes higher and thinner as V increases from 2 to 20 m/s (K = 177–17,720). From the experimental observations conducted by Okawa et al. [10], the lower boundaries for the crown formation and for the production of secondary drops are expressed by K = 700 and 2,100, respectively. Hence, the numerical results depicted in Fig. 3a appear consistent with the experimental results. Depicted in Fig. 3b is the effect of film thickness. When η = 0.5, the calculated interfacial shape is almost identical to that for $\eta = 1$ shown at right in Fig. 2b. It is worth noting in these two cases that a part of liquid originally included in the inner region of crown is transported to the outer region. As a result, the base region of outer wall of crown is rounded noticeably. However, if η is further decreased, the liquid transport is limited due to the reduction of the gap distance connecting the inner and outer regions. Consequently, the crown wall becomes thinner with a decrease in η. In particular, one finds that the outer wall of crown becomes almost flat when η is reduced to 0.05.

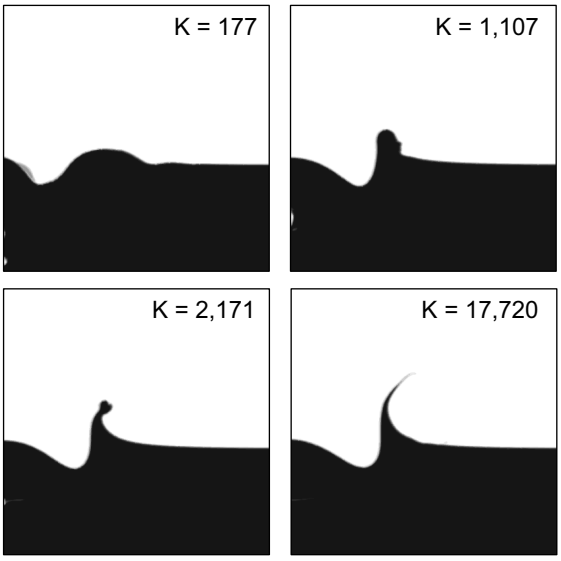

(a) Effect of impact velocity when h = 0.4 mm ($\eta = 1$)

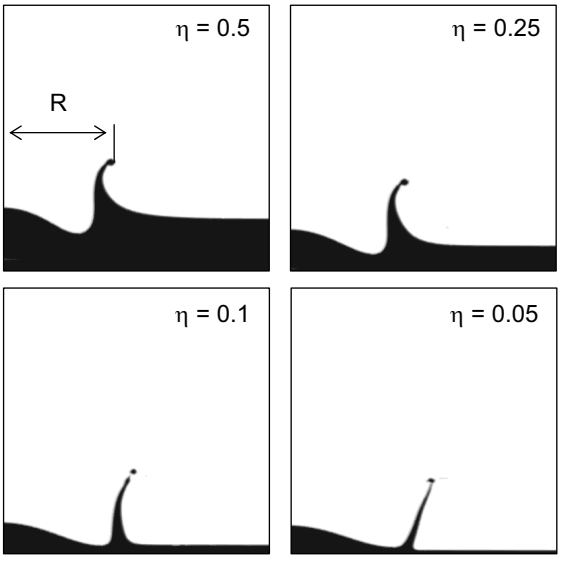

(b) Effect of film thickness when V = 10 m/s (K = 4,430)

Fig. 3: Calculated interfacial shapes at $\tau = 1$.

Crown radius

The time evolution of crown radius R was measured for several cases; here, to minimize the measurement uncertainty, R was defined as the outer radius of crown rim as shown at upper left in Fig. 3b. The effects of V and h on R are displayed in Figs. 4a and b, respectively. Josserand and Zaleski [19] and Rieber and Frohn [18] showed numerically that the time evolution of crown size is expressed by $R/d = k\tau^{1/2}$ and the proportionality factor k is not dependent on We and Re; here, the Reynolds number Re is defined by $Re = \rho Vd/\mu$. In these simulations, η was rather small and within 0.1–0.15. Figure 4a indicates that V does not influence the time evolution of R. This is consistent with the previous numerical results. However, though R/d is roughly proportional to $\tau^{1/2}$ in the early stage as in the case of previous simulations, the radial propagation of crown is slightly slowed down in the later stage ($\tau > 0.3$) in the present simulations. Figure 4b shows that this gradual decrease in the propagation speed of crown is not observed when the liquid film is sufficiently thin (η = 0.05 and 0.025).

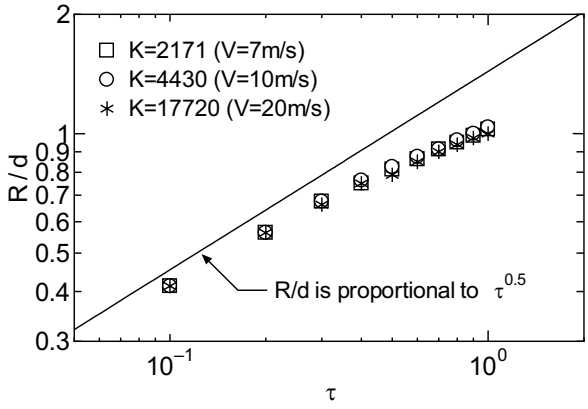

(a) Effect of impact velocity

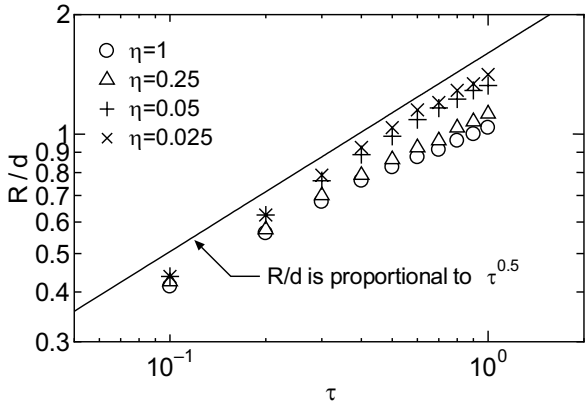

(b) Effect of film thickness

Fig. 4: Time evolution of the outer radius of crown rim.

Maximum pressure

Time evolution of the spatial distribution of dimensionless pressure $\Pi = (P–P_0)/\rho V^2$ calculated in the reference case is depicted in Fig. 5. The local pressure is highest around the impact neck in the early stage as in the numerical simulations by Josserand and Zaleski [19]. Time evolutions of the peak pressure in liquid $\Pi_{l,max}$ and the peak pressure on the bottom wall $\Pi_{b,max}$ calculated under three analytical conditions are shown in Figs. 6a and b, respectively. It can be seen in Fig. 6a that $\Pi_{l,max}$ is proportional to $\tau^{-1/2}$ in the initial stage and then

drops more rapidly. This is consistent with the theory and numerical results reported by Josserand and Zaleski [19]. Comparing the results for $K = 4{,}430$ and 17,720 reveals that the start time of the rapid decrease of $\Pi_{l,max}$ is not influenced by V, but the result for $\eta = 0.05$ shows that the rapid decrease commences later when h is smaller. Consequently, the difference in $\Pi_{l,max}$ due to η is greater in the later stage ($\tau > 0.2$). Figure 6b indicates that $\Pi_{b,max}$ is almost equal to $\Pi_{l,max}$ in the case of thin liquid film ($\eta = 0.05$) since the impact neck is formed in the close vicinity of the bottom wall. On the other hand, in the cases of thicker films ($\eta = 1$), $\Pi_{b,max}$ is much smaller than $\Pi_{l,max}$ in the early stage. Though $\Pi_{b,max}$ increases gradually, it can be confirmed that the maximum pressure applied to the bottom wall is reduced significantly if η is sufficiently large.

To show the effects of V and h on the peak pressure quantitatively, the peak pressures at $\tau = 0.2$ are plotted against K and η in Figs. 7a and b, respectively. It can be confirmed in Fig. 7a that both the dimensionless peak pressures in liquid and on the bottom wall are not dependent on K. This implies that $P–P_0$ is fairly proportional to ρV^2. Figure 7b shows that $\Pi_{l,max}$ decreases with an increase in η. It is however interesting to note that the dependence of $\Pi_{l,max}$ on η is less significant for thin films of $\eta < 0.1$ and for thick films of $\eta > 0.5$. If the liquid originally included in the inner region of crown is transported to the outer region, the pressure rise caused by the drop impact is mitigated. It is hence considered that the liquid transport is nearly negligible when $\eta < 0.1$ while maximized when $\eta > 0.5$. From this perspective, the boundary between thin and thick films is present around $\eta = 0.25$. Figure 7b also indicates that $\Pi_{b,max}$ is equal to $\Pi_{l,max}$ for thin films ($\eta < 0.25$), but the deviation of $\Pi_{b,max}$ from $\Pi_{l,max}$ becomes significant with an increase in η for thick films ($\eta > 0.5$).

With an increase in the film thickness, the maximum impact pressure in liquid decreases and the difference between the maximum pressures in liquid and on the bottom wall increases. These are regarded as the main mechanisms of the mitigation of the maximum impact pressure on the bottom wall when the liquid film is thick.

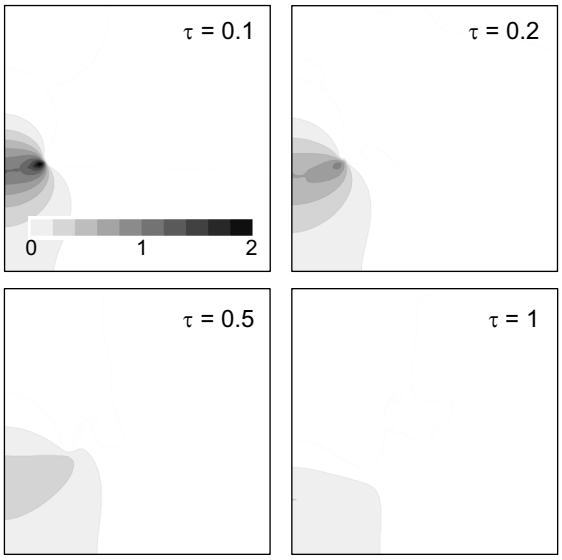

Fig. 5: Time evolution of the spatial distribution of dimensionless pressure in units of ρV^2.

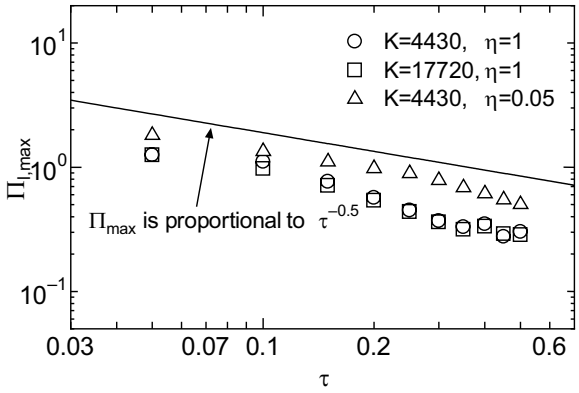

(a) Peak pressure in liquid

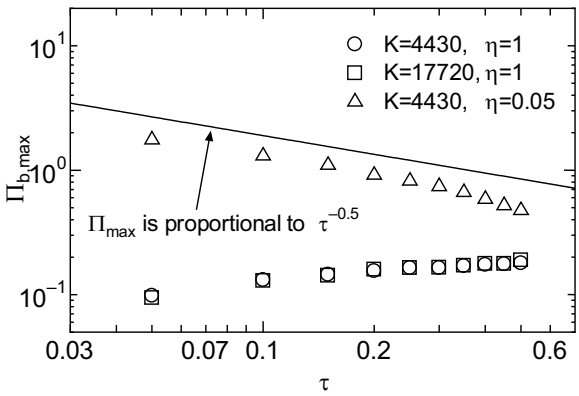

(b) Peak pressure on the bottom wall

Fig. 6: Time evolutions of pressure peak.

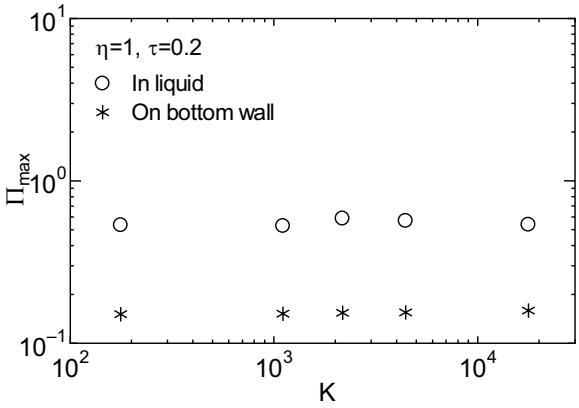

(a) Effect of impact velocity

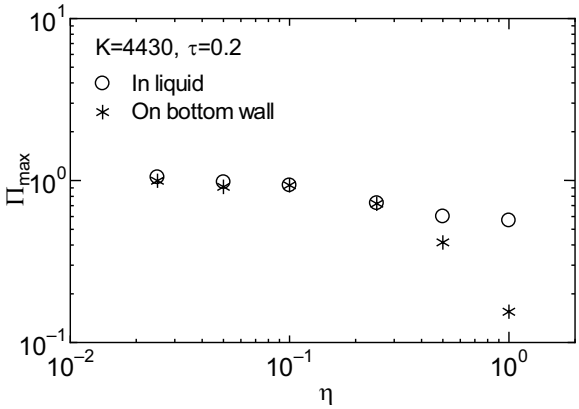

(b) Effect of film thickness

Fig. 7: Pressure peak at $\tau = 0.2$.

Maximum jet velocity

Displayed in Fig. 8 is the temporal evolution of dimensionless liquid velocity $\varsigma_l = V_l/V$ calculated in the reference case. In the early stage, the maximum velocity $\varsigma_{l,max}$ is measured within the liquid jet formed at the impact neck. Figure 9 shows the maximum liquid velocity $\varsigma_{l,max}$ as a function of time. It can be seen that $\varsigma_{l,max}$ decreases in proportion to $\tau^{-1/2}$ under all the three analytical conditions. This dependence of $\varsigma_{l,max}$ on τ agrees with the simple theory by Josserand and Zaleski [19] in which viscous effect is neglected. It should however be noted that, in the initial stage of $\tau < 0.2$, this relation between τ and $\varsigma_{l,max}$ cannot be confirmed in Fig. 9. This is because the computational cells used in the present simulations are not fine enough to resolve very small initial jet accurately. It is also seen in Fig. 9 that $\varsigma_{l,max}$ is not influenced by V but decreases with h. The values of $\varsigma_{l,max}$ measured at $\tau = 0.2$ are plotted against K and η in Figs. 10a and b, respectively. The dependences of $\varsigma_{l,max}$ on K and η are similar to those of $\Pi_{l,max}$ shown in Fig. 7; namely, $\varsigma_{l,max}$ is not influenced significantly by K while decreases with an increase in η. The effect of η is particularly noticeable around $\eta = 0.25$. This also indicates that the liquid film can be regarded as a thin film if η is less than about 0.25 in the sense that the bottom wall affects the crown behavior.

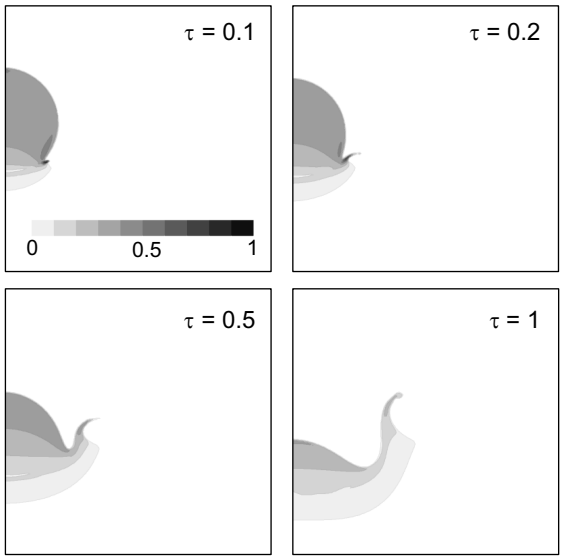

Fig. 8: Time evolution of the spatial distribution of dimensionless liquid velocity in units of V.

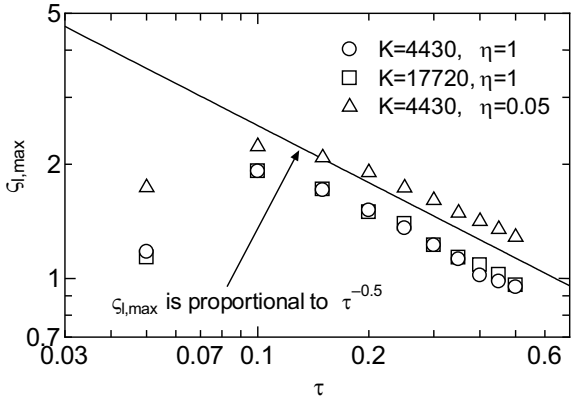

Fig. 9: Time evolutions of maximum liquid velocity.

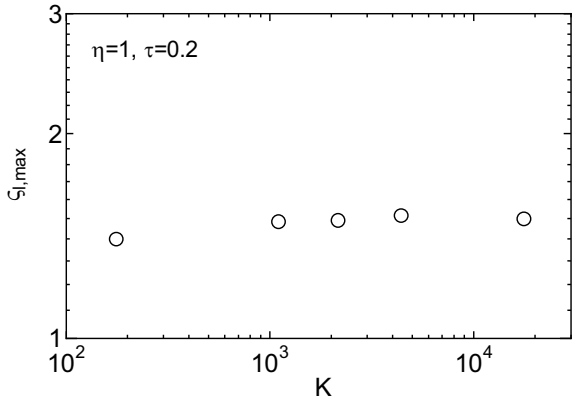

(a) Effect of impact velocity

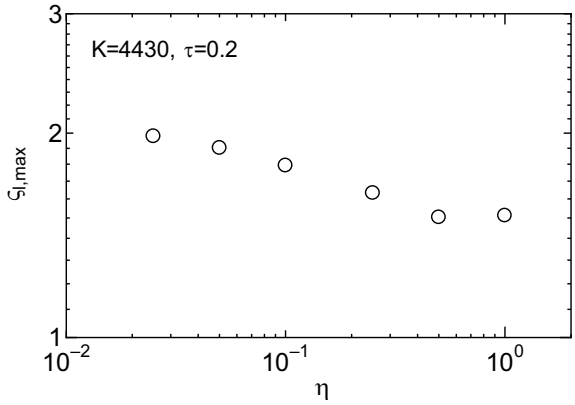

(b) Effect of film thickness

Fig. 10: Maximum liquid velocity at $\tau = 0.2$.

Role of liquid transport to the outer region

From the present numerical results, it is considered that the liquid transport from the inner to outer regions of liquid crown is the key phenomena to interpret the effect of film thickness. Since the gap distance connecting the inner and outer regions is larger when the liquid film is thicker, the liquid can travel more freely between the two regions in this case. More liquid was hence transported to the outer region and consequently the base region of outer wall of crown was rounded noticeably as depicted in Fig. 3b when the liquid film was thick. The gradual decrease of the propagation speed of liquid crown shown in Fig. 4a can hence be attributed to the transported liquid since it would act as the inertia added to the liquid crown. If the liquid is transported to the outer region, the liquid film would act as a buffer material against the drop impact. Therefore, the decreases of impact pressure and jet velocity with an increase in the film thickness that were depicted in Figs. 7b and 10b can also be understood as a consequence of the liquid transport.

EFFECT OF IMPINGEMENT ANGLE

Interfacial shape

The effect of impingement angle α on the calculated time evolution of the interfacial shape is depicted in Fig. 11. In these simulations, d and h were set to 0.4 mm; the normal component of initial drop velocity V_n was kept at 10 m/s while the tangential component V_t (= $V_n \tan\alpha$) was changed parametrically. Shown in Fig. 11a are the calculated results for normal impact. It is noted that the crown size is greater in this figure than in Fig. 2 since the cylindrical drop of larger inertia

was used. However, the crown shapes are fairly similar to those calculated for a spherical drop. Though the two liquid sheets are almost identical in the case of normal impact (Fig. 11a), they are significantly different in the cases of oblique impact (Figs. 11b and c). In the latter two cases, since the impacting drop presses the base of right side liquid sheet, the maximum pressure is measured in this region (see Fig. 12a). In addition, the jet velocity is higher in the right side sheet than in the left side one as shown in Fig. 12b since the liquid originally included in the impacting drop flows directly into the right side liquid sheet. Comparing Figs. 11b and c indicates that the difference between the right and left side sheets in the earlier stage ($\tau < 0.2$) becomes significant with an increase in α. Another interesting observation in Fig. 11 is the effect of α on the ejection angle of the right side liquid sheet. It can be seen at $\tau = 0.2$ that the angle between the liquid sheet and the horizontal surface decreases with an increase in α. This can be attributed to the increase of the tangential component of the impact velocity with α. In particular, though the liquid sheet is directed upward when $\alpha = 0$ and 30º, it is directed downward when $\alpha = 60$º. As a result, the liquid sheet is then elongated when $\alpha = 0$ and 30º but the sheet elongation is restricted when

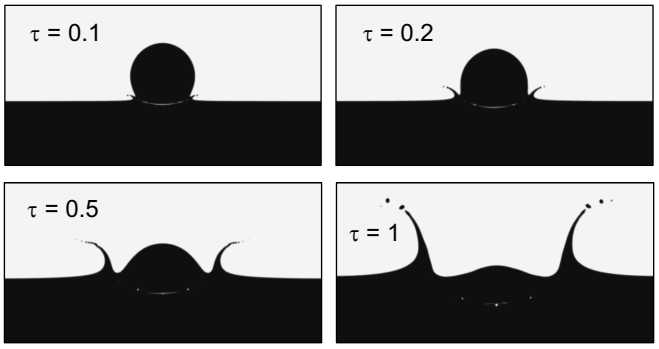

(a) $\alpha = 0$º

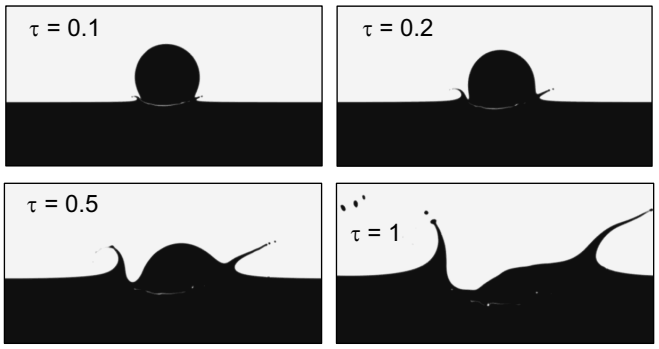

(b) $\alpha = 30$º

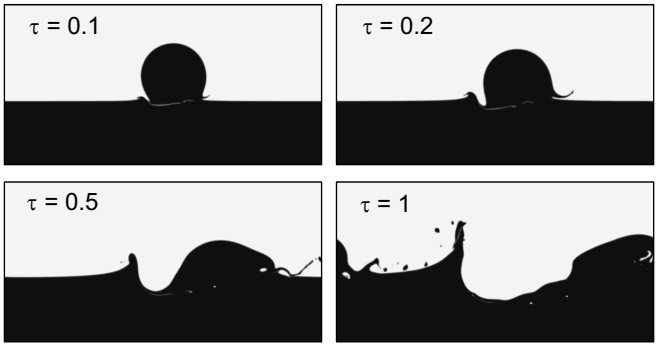

(c) $\alpha = 60$º

Fig. 11: Effect of impingement angle α on the calculated time evolution of the interfacial shape.

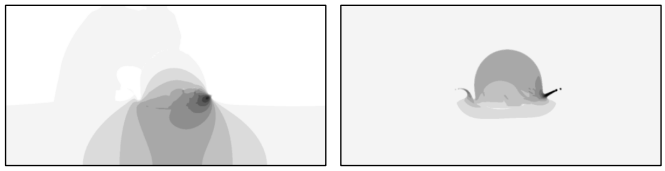

(a) Pressure field (b) Liquid velocity field

Fig. 12: Spatial distributions of pressure and liquid velocity at $\tau = 0.2$ when $\alpha = 30$º.

$\alpha = 60$º since the sheet collides with a liquid film surface. Okawa et al. [11] reported the experimental result that the formation of liquid sheet and the production of secondary drops become rare events in very oblique impacts of $\alpha >$ 50–70º. The present numerical results indicate that the reduction of the ejection angle of liquid sheet with an increase in α would be a main cause of this experimental observation.

Maximum pressure and maximum jet velocity

The effects of α on the maximum values of pressure and liquid velocity were investigated using the present numerical results. The normal component V_n and the total momentum vector V were kept at 10 m/s in the first and second series of simulations, respectively; α was changed parametrically within 0–70º in both the series. The maximum values were measured at $\tau = 0.2$.

The dimensionless maximum pressures $\Pi_{n,max}$ and Π_{max} are defined respectively by

$$\Pi_{n,max} = (P_{max} - P_0)/\rho V_n^2 \quad (1)$$

$$\Pi_{max} = (P_{max} - P_0)/\rho V^2 \quad (2)$$

The dependence of $\Pi_{n,max}$ on α is shown in Fig. 13a. It can be seen that the values of $\Pi_{ln,max}$ (in liquid) and $\Pi_{bn,max}$ (on bottom wall) vary only slightly between the first and second series. This confirms that ρV_n^2 or ρV^2 is the appropriate scaling parameter of pressure even for the oblique impacts. However, $\Pi_{ln,max}$ increases monotonously with an increase in α. This implies that not only V_n but also V_t is influential in determining the maximum pressure in liquid. In the simulations of oblique impact, the maximum pressure was measured at the base of the right side liquid sheet as depicted in Fig. 12a. One can hence confirm that the lateral velocity component is the cause of the rise of local pressure. The maximum dimensionless pressures measured on the bottom wall $\Pi_{bn,max}$ are also plotted in Fig. 13a. Contrary to $\Pi_{ln,max}$, $\Pi_{bn,max}$ is not influenced significantly by α if α is smaller than 45º. This indicates that the pressure rise induced by the tangential component is less penetrative to the liquid film. However, $\Pi_{bn,max}$ also increases with an increase in α when α is greater than 45º. It is hence concluded that the effect of the tangential component is not necessarily negligible in determining the erosion damage induced by the drop impact. The scaling parameter of pressure rise is changed from ρV_n^2 to ρV^2 in Fig. 13b. It is found that $\Pi_{l,max}$ is fairly constant if α is not very large ($\alpha <$ 45º). It is hence considered that the maximum local pressure is dominated by V rather than V_n. However, $\Pi_{l,max}$ decreases with an increase in α when α is greater than 45º. This indicates that the contribution of V_t to the pressure rise becomes less significant in very oblique impact.

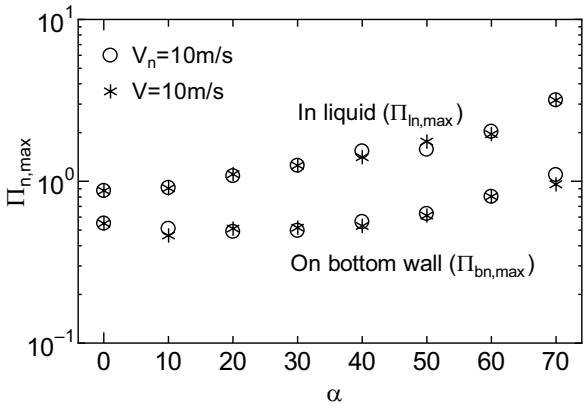

(a) Effect of α (P is scaled by ρV_n^2)

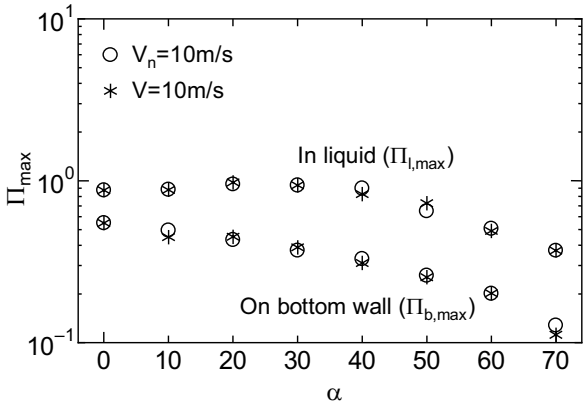

(b) Effect of α (P is scaled by ρV^2)

Fig. 13: Pressure peak at $\tau = 0.2$.

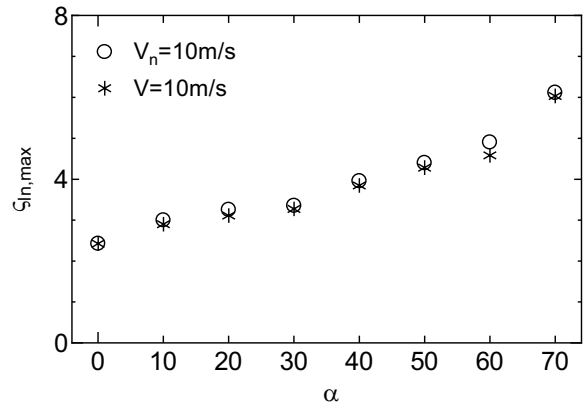

(a) Effect of α (V_l is scaled by V_n)

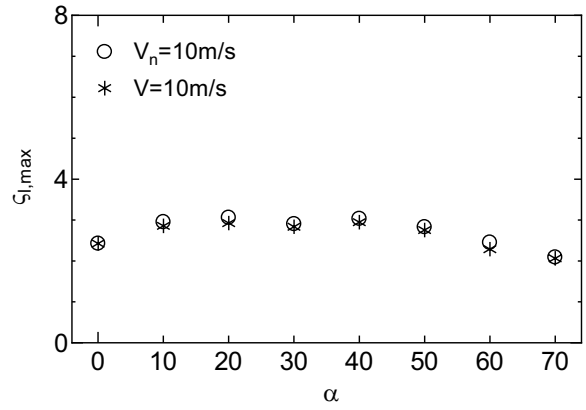

(b) Effect of α (V_l is scaled by V)

Fig. 14: Maximum liquid velocity at $\tau = 0.2$.

The dependence of the maximum liquid velocity on α is displayed in Figs. 14a and b. Here, the dimensionless maximum velocities $\varsigma_{ln,max}$ and $\varsigma_{l,max}$ are defined respectively by

$$\varsigma_{fn,max} = V_{l,max} / V_n \tag{3}$$

$$\varsigma_{fn,max} = V_{l,max} / V \tag{4}$$

Since the maximum liquid velocity was measured within the right side liquid jet as depicted in Fig. 12b, the maximum liquid velocity is identical to the maximum jet velocity. Figures 14a and b indicate that $\varsigma_{ln,max}$ increases monotonously with an increase in α while $\varsigma_{l,max}$ is not influenced significantly by α. It is hence considered that liquid jet properties are primarily determined by the total momentum vector V rather than the normal component V_n in the case of oblique drop impact. Okawa et al. [11] showed experimentally that the critical value of K at the deposition-splashing limit is expressed by the following correlation if $\alpha < 50°$:

$$K = WeOh^{-0.4} = 2{,}100 \tag{5}$$

Since not V_n but V is used in calculating We in the above correlation, the present conclusion is consistent with the above experimental result.

CONCLUSIONS

Systematic two-dimensional interface tracking simulations were carried out to elucidate the effect of several important parameters on the process of single drop impingement onto a plane liquid film. Main conclusions of this numerical work are summarized as:

(1) When the target liquid film was thick, the part of liquid originally included in the inner region of crown was transported to the outer region. As a result, the base region of outer wall of liquid crown was rounded noticeably. In the case of thin liquid film, however, the liquid transport was negligibly small since the gap distance connecting the inner and outer regions was small. Due to the presence of liquid transport, the following observations were made for thick films: (a) the propagation speed of liquid crown was gradually slowed down since the transported liquid acted as the inertia added to the liquid crown, (b) the maximum pressure at the impact neck and the maximum velocity within the liquid jet decreased since the liquid film played a role as the buffer material against the drop impact. It is hence inferred that the production of secondary drops is mitigated in the case of thick film since the liquid crown is stabilized.

(2) The pressure rise on the bottom wall caused by the drop impact became less significant with an increase in the target liquid film thickness. The mitigation of pressure rise was attributed to the decrease of the maximum pressure measured at the impact neck and to the increase of the pressure difference between the impact neck and the bottom wall. It is expected that the erosion damage of solid material induced by the drop impact can be significantly mitigated if the impacted wall is covered with the liquid film whose thickness is comparable to the drop diameter.

(3) In the case of oblique impact, the impacting drop pressed the target liquid film laterally. Hence, the tangential as well as the normal components of the impact velocity was

influential in determining the maximum pressure and the jet velocity. However, when the impingement angle was not very large, the effects of impingement angle on the pressure at the impact neck and the jet velocity were not significant provided that the total momentum vector of impact velocity was selected as the scaling parameter of velocity. This is consistent with the available experimental observation that not the normal component but the total momentum vector of impact velocity is roughly constant at the deposition-splashing limit.

(4) When the impingement angle was very large, the liquid jet directed downward and eventually collided with the surface of target liquid film, which prevented the further elongation of liquid jet. This is considered one of the main reasons why the formation of liquid sheet and the production of secondary drops become rare events when the impingement angle is very large.

NOMENCLATURE

d	primary drop diameter	m
h	Film thickness	m
K	impact K-number	dimensionless
Oh	Ohnesorge number	dimensionless
P	pressure	Pa
P_0	reference pressure	Pa
R	crown radius	m
V	impact velocity	m/s
V_l	liquid velocity	m/s
We	impact Weber number	dimensionless

Greek symbols

α	impingement angle	degree
Δx	mesh size	m
η	dimensionless film thickness	dimensionless
μ	liquid viscosity	Pa·s
Π	dimensionless pressure	dimensionless
ρ	liquid density	kg/m^3
σ	surface tension	N/m
τ	dimensionless time	dimensionless
ς	dimensionless velocity	dimensionless

Subscripts

b	bottom wall
l	liquid
max	maximum
n	normal to film surface
t	tangential to film surface

REFERENCES

[1] A. M. Worthington, A study of splashes, Macmillan, New York (1963).

[2] M. Rein, Phenomena of liquid drop impact on solid and liquid surfaces, *Fluid Dynamics Research*, vol. 12, pp. 61-93 (1993).

[3] A. Prosperetti, H. N. Oguz, H. N., The impact of drops on liquid surfaces and the underwater noise of rain, *Annual Review of Fluid Mechanics*, vol. 25, pp. 577-602 (1993).

[4] A. L. Yarin, Drop impact dynamics: splashing, spreading, receding, bouncing..., *Annual Review of Fluid Mechanics*, vol. 38, pp. 159-192 (2006).

[5] H. Xie, S. Koshizuka, Y. Oka, Numerical simulation of liquid drop deposition in annular-mist flow regime of boiling water reactor, *Journal of Nuclear Science and Technology*, vol. 41, pp. 569-578 (2004).

[6] A. L. Yarin, D. A. Weiss, Impact of drops on solid surfaces: self-similar capillary waves, and splashing as a new type of kinematic discontinuity, *Journal of Fluid Mechanics*, vol. 283, pp. 141-173 (1995).

[7] G. E. Cossali, A. Coghe, M. Marengo, The impact of a single drop on a wetted solid surface, *Experiments in Fluids*, vol. 22, pp. 463-472 (1997).

[8] A. B. Wang, C. C. Chen, Splashing impact of a single drop onto very thin liquid films, *Physics of Fluids*, vol. 12, pp. 2155-2158 (2000).

[9] R. Rioboo, C. Bauthier, J. Conti, M. Voue, J. D. Coninck, Experimental investigation of splash and crown formation during single drop impact on wetted surfaces, *Experiments in Fluids*, vol. 35, pp. 648-652 (2003).

[10] T. Okawa, T. Shiraishi, T. Mori, Production of secondary drops during the single water drop impact onto a plane water surface, *Experiments in Fluids*, vol. 41, pp. 965-974 (2006).

[11] T. Okawa, T. Shiraishi, T. Mori, Effect of impingement angle on the outcome of single water drop impact onto a plane water surface, *Experiments in Fluids*, vol. 44, pp. 331-339 (2008).

[12] T. Okawa, More on the droplet deposition in annular two-phase flow, *Proceedings of 6th International Conference on Multiphase Flow*, Leipzig, Germany, Paper No. KN-8 (2007).

[13] P. I. A. Kinnell, Raindrop-impact-induced erosion processes and prediction: a review, *Hydrological Process*, vol. 19, pp. 2815-2844 (2005).

[14] G. Erpul, D. Gabriels, L. D. Norton, Sand detachment by wind-driven raindrops, *Earth Surface Processes and Landforms*, vol. 30, pp. 241-250 (2005).

[15] Y. I. Oka, S. Mihara, H. Miyata, Effective parameters for erosion caused by water droplet impingement and applications to surface treatment technology, *Wear*, vol. 263, pp. 386-394 (2007).

[16] F. H. Harlow, J. P. Shannon, The splash of a liquid drop, *Journal of Applied Physics*, vol. 38, pp. 3855-3866 (1967).

[17] H. N. Oguz, A. Prosperetti, Bubble entrainment by the impact of drops on liquid surfaces, *Journal of Fluid Mechanics*, vol. 219, pp. 143-179 (1990).

[18] M. Rieber, A. Frohn, A numerical study on the mechanism of splashing, *International Journal of Heat and Fluid Flow*, vol. 20, pp. 455-461 (1999).

[19] C. Josserand, S. Zaleski, Droplet splashing on a thin liquid film, *Physics of Fluids*, vol. 15, pp. 1650-1657 (2003).

[20] N. Nikolopoulos, A. Theodorakakos, G. Bergeles, Three-dimensional numerical investigation of a droplet impinging normally onto a wall film, *Journal of Computational Physics*, vol. 225, pp. 322-341 (2007).

[21] S. F. Lunkad, V. V. Buwa, K. D. P. Nigam, Numerical simulations of drop impact and spreading on horizontal and inclined surfaces, *Chemical Engineering and Science*, vol. 62, pp. 7214-7224 (2007).